Electronic Supplementary Information:

Triggered micropore-forming bioprinting of porous viscoelastic hydrogels

Guangyu Bao,[a] Tao Jiang,[a] Hossein Ravanbakhsh,[a] Alicia Reyes,[ab] Zhenwei Ma,[a] Mitchell Strong,[a] Huijie Wang,[a] Joseph M. Kinsella,[c] Jianyu Li*[ab] and Luc Mongeau*[a]

[a]Department of Mechanical Engineering, McGill University, Montreal, QC H3A 0C3, Canada

[b]Department of Biomedical Engineering, McGill University, Montreal, QC H3A 0C3, Canada

[c]Department of Bioengineering, McGill University, Montreal, QC H3A 0C3, Canada

*Correspondence and requests for materials should be addressed to J.L. (jianyu.li@mcgill.ca) or L.M. (luc.mongeau@mcgill.ca).

List of supporting information:

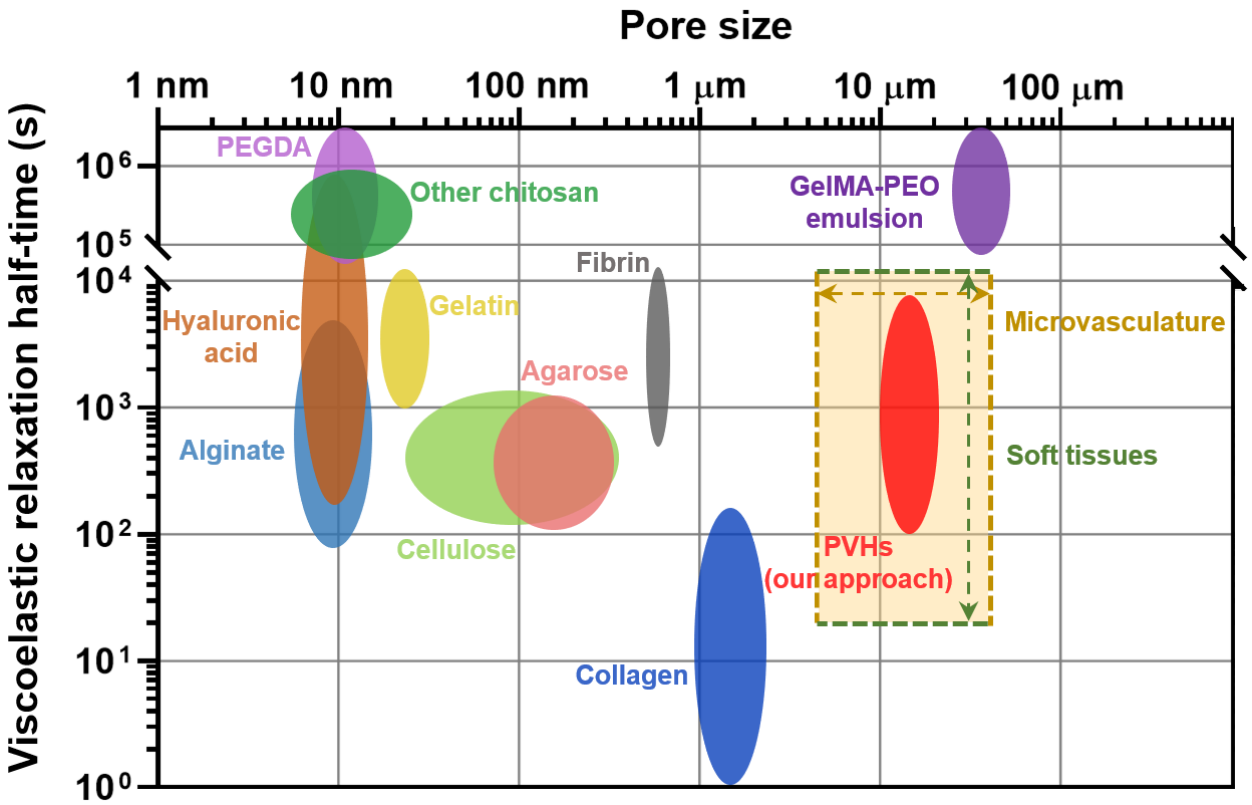

Figure S1 Pore size and stress relaxation timescale of various bioprinting materials. The stress relaxation timescale is defined at the time period for the stress to relax to one-half of its initial value under a constant strain. Pores larger than 100 μm are achievable using direct bioprinting and other scaffold fabrication techniques. Refs: agarose[38,39], alginate[40–42], cellulose[43–45], other chitosan[46], collagen[47,48], fibrin[49,50], gelatin[51,52], GelMA-PEO emulsion[15], hyaluronic acid[53,54], PEGDA[5,49], microvasculature[55,56], and soft tissues[20,42,57,58].

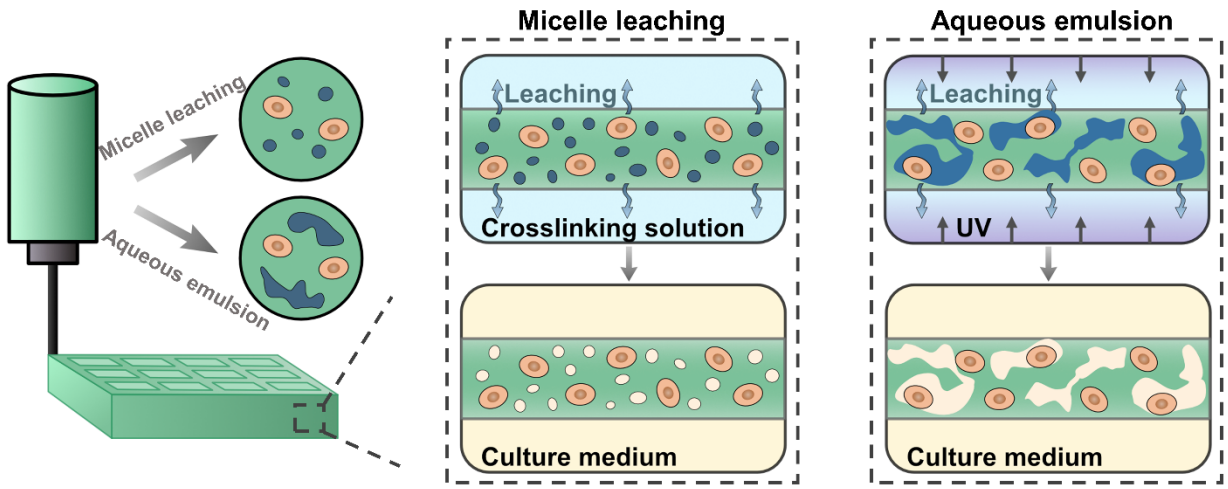

Figure S2 Current strategies for bioprinting hydrogels with micropores.

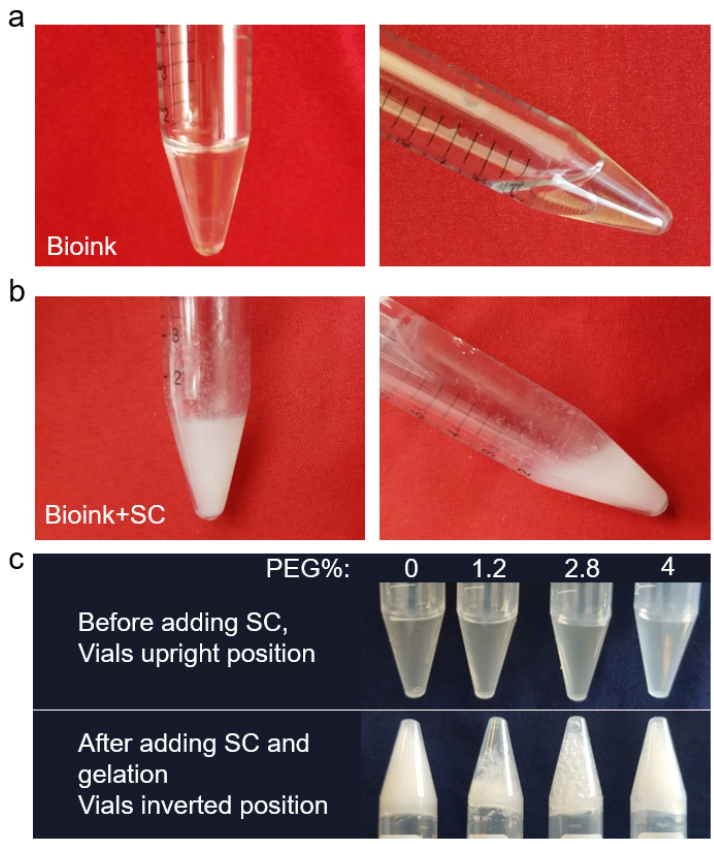

Figure S3 Digital photos of bioinks before and after mixing with a phase-separation inducing agent, sodium bicarbonate (SC). (a) Bioink consists of 1.5 wt% chitosan, 0.12 M acetic acid and 0.04 M phosphate salts. The bioink is fully transparent and stable at room temperature. (b) Bioink mixed with a phase-separation inducing agent (0.184 M sodium bicarbonate) at a final pH of 6.8. Upon mixing, the mixture forms micro-phase separation and weak crosslinks, resulting in a translucent gel and suspended flocs attached to the vial wall. The bioinks formed opaque physically-crosslinked hydrogels and do not flow when the vials are in the upside-down positions. (c) Bioinks with varying PEG contents before (upper) and after (lower) adding SC. Opaque gels are formed in inverted vials, indicative of sol-gel transition.

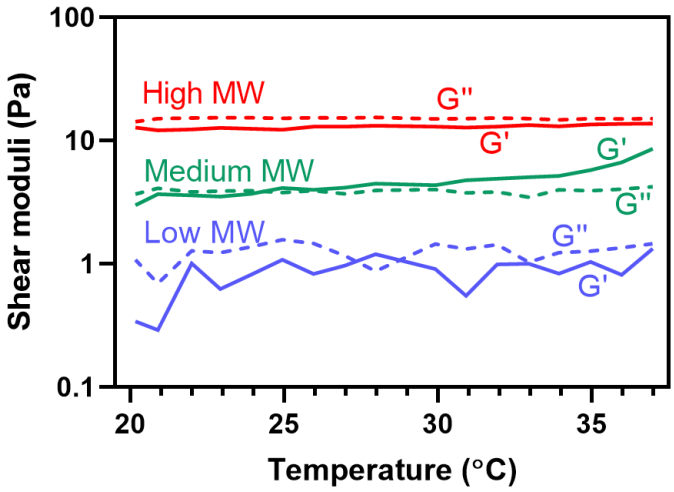

Figure S4 Temperature sweep of chitosans with low deacetylation degree (DDA 75-85%) and varying molecular weights. G' and G'' refer to storage and loss modulus, respectively. No thermal gelation is observed at 37℃.

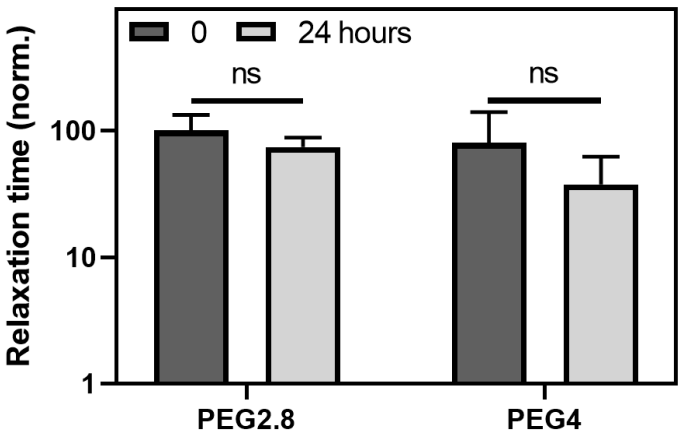

Figure S5 Relaxation stability for PEG2.8 and PEG4 hydrogels. The relaxation time maintained the same after the hydrogels were fully immersed inside complete DMEM + 10% FBS cell culture medium for 24 hours at 37℃.

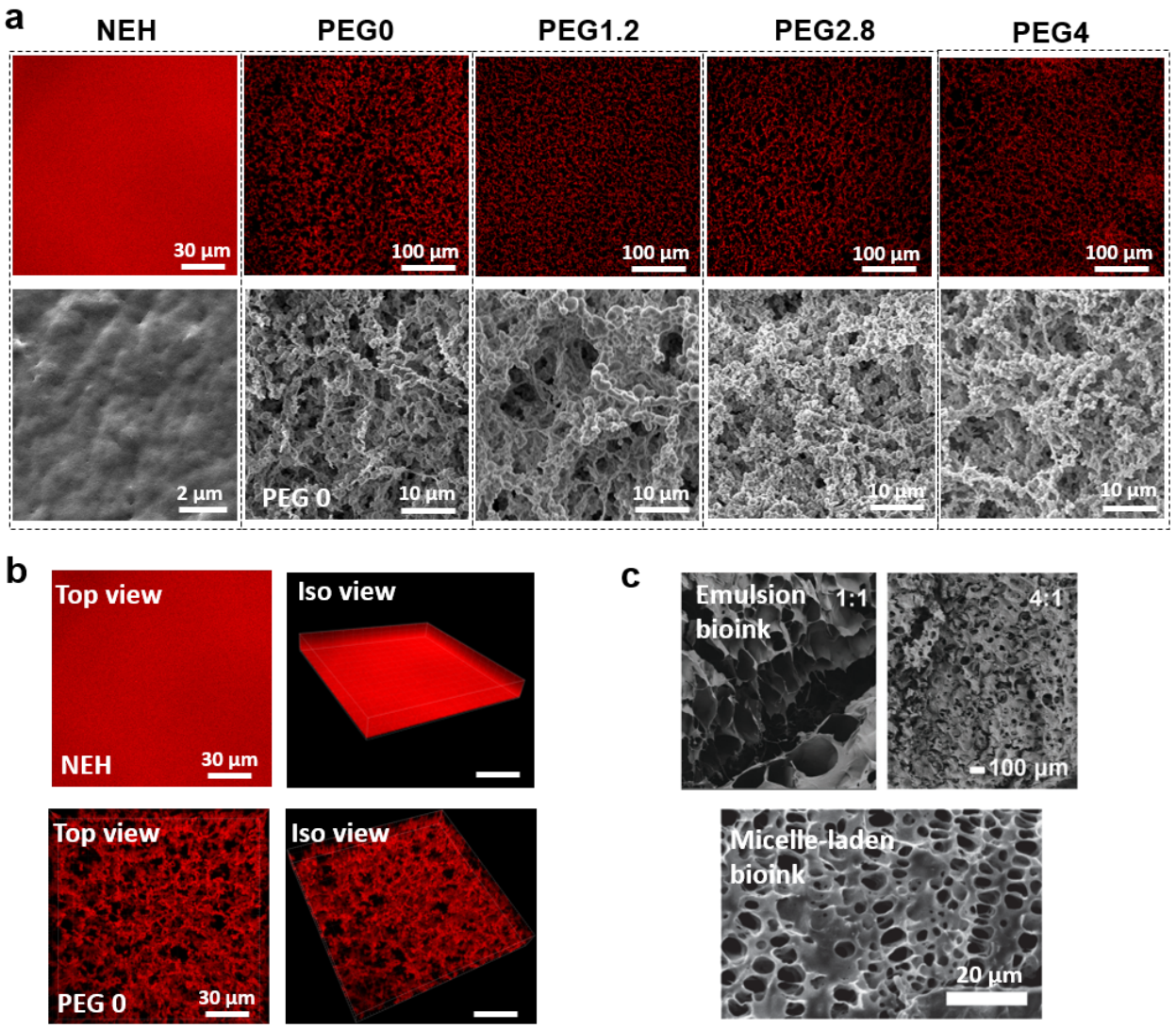

Figure S6 Microstructures of the polymeric networks of PVHs and NEHs. Rhodamine-B labeled chitosan is used for confocal imaging. The control is NEH, glyoxal crosslinked glycol-chitosan and unmodified chitosan. (a) Confocal and SEM images of PVH show highly interconnected micropores, while no micropores are observed in NEH. (b) Reconstruction of the 3D structure of NEH and PVH from confocal z-stack images. (c) Porous structure of hydrogels fabricated using emulsion[15] and micelle-laden[14] bioinks. The pore interconnectivity is lower compared to that of PVHs (images reproduced with permissions).

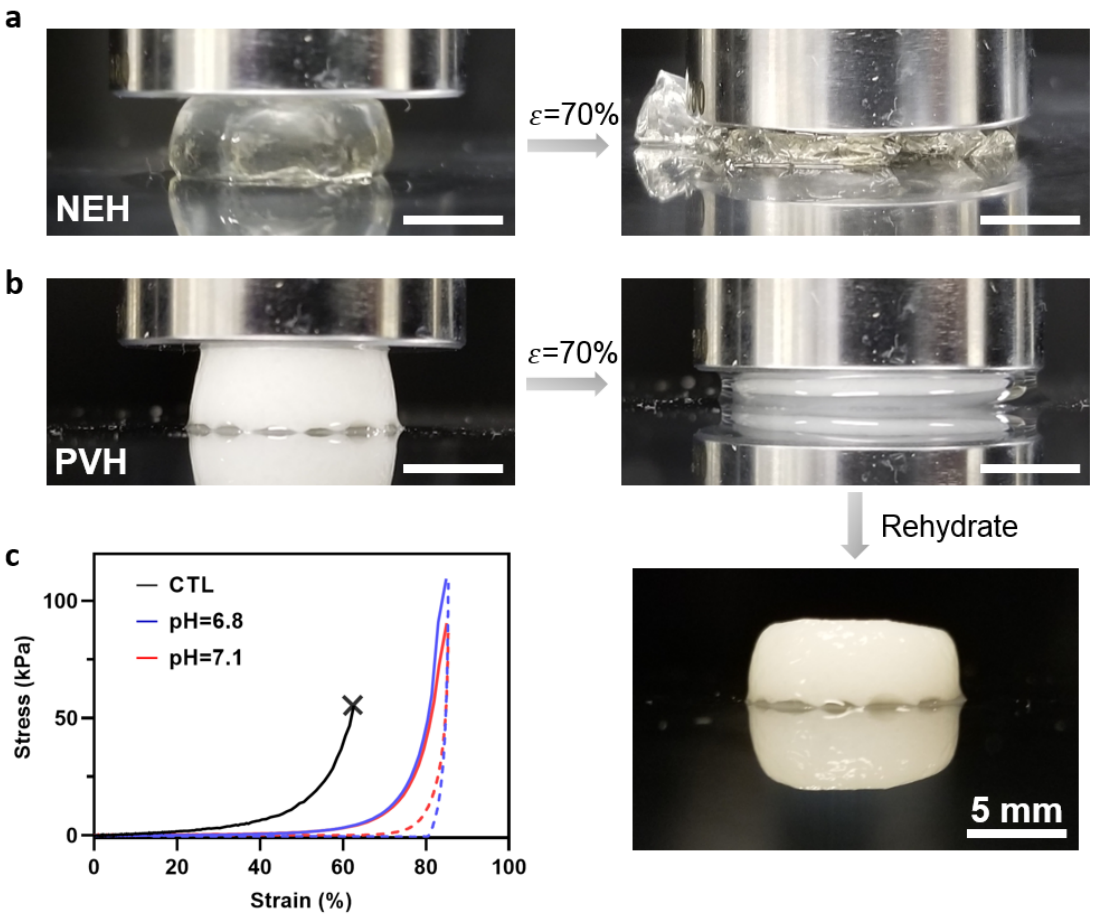

Figure S7 Compression tests on PVHs and NEHs. (a) Digital images showing compression tests on NEH with 70% strain. NEH ruptures during the compression. (b) Digital images showing compression tests on PVH with 70% strain. Water migrates out of PVH during the compression and PVH doesn't rupture. Compressed PVH resumes to its original shapes after 30 mins of rehydration inside PBS. (c) Load-unloading curves for compression tests with 85% strain. Sample size, N=3; scale bar 5mm.

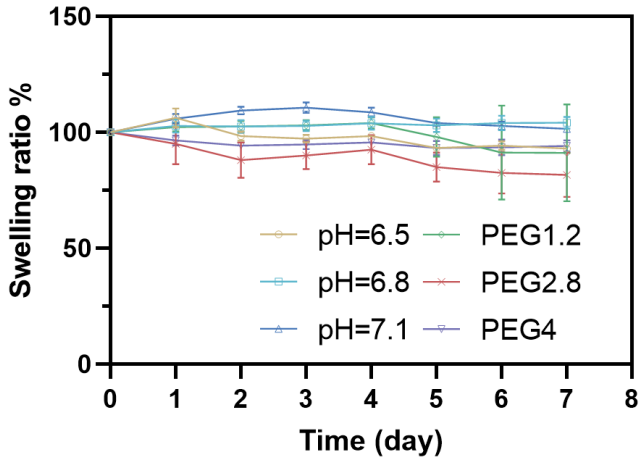

Figure S8 Swelling profiles of PVHs in PBS. The swelling ratio of the gels, which are formed with varying pH and PEG conditions, is measured based on the mass change. No significant swelling is observed in the tested PVHs. Error bars indicate standard deviation; Sample size, N=3.

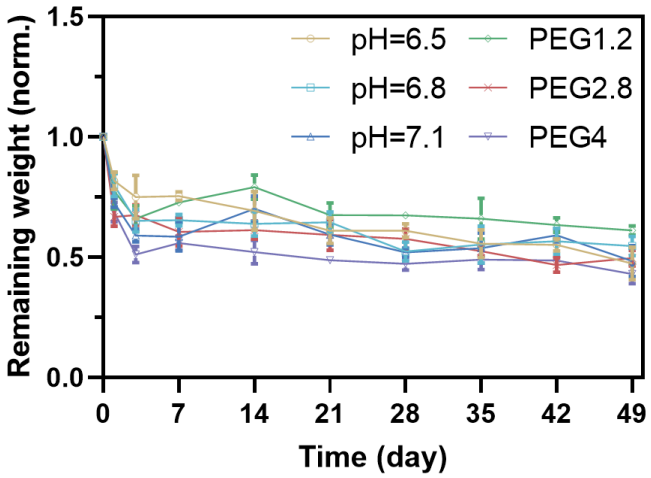

Figure S9 Extended degradation profiles of PVHs synthesized at varying pH and PEG conditions. The gels are exposed to lysozyme enzyme (13 µg/ml) in PBS for 7 weeks. The remaining weight is calculated by normalizing the dry mass of the gel with its initial dry mass before degradation. All the conditions lead to similar degradation profiles. Error bars indicate standard deviation; Sample size, N=3.

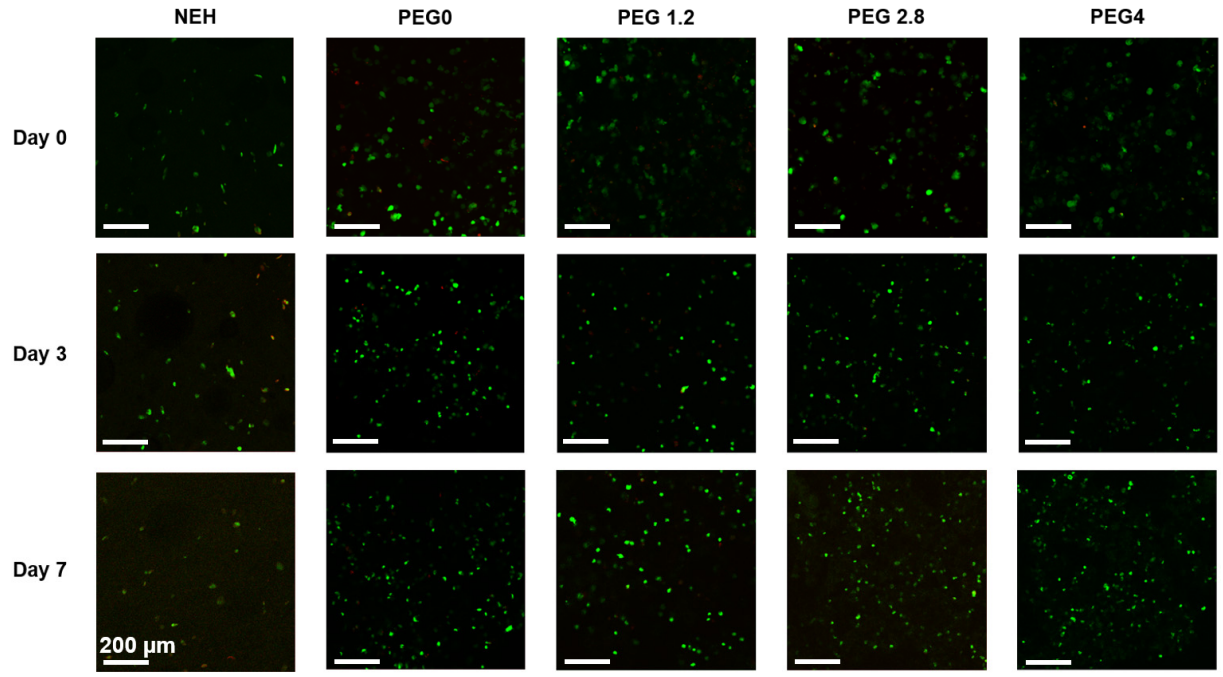

Figure S10 Fluorescent images of live/dead cells cultured within hydrogels. Live cells are in green and dead cells in red. Sample size, N=5.

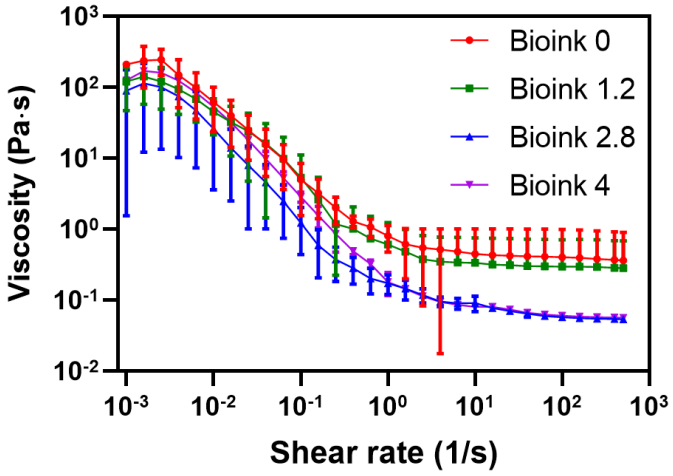

Figure S11 Viscosity curves of bioinks containing varying concentrations of polyethylene glycol (PEG). The legend, bioink xx, denotes the concentration of PEG within the bioink. Error bars indicate standard deviation; Sample size, N=3.

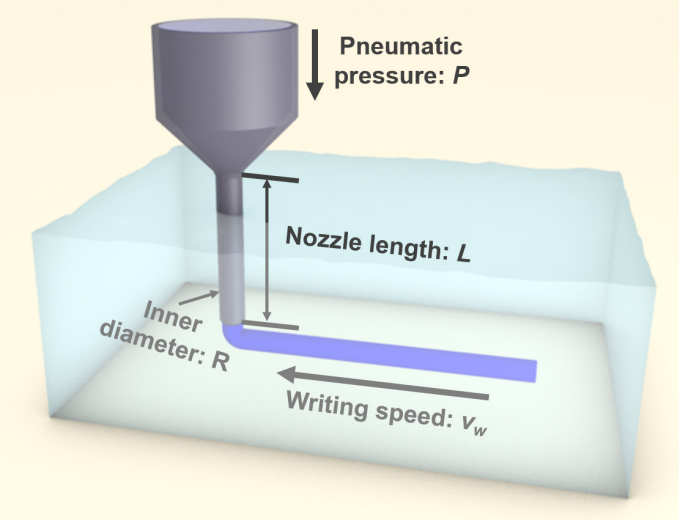

Figure S12 Schematic of cell-laden bioink passing through a cylindrical nozzle into a supportive matrix.

For embedded extrusion bioprinting where the extrusion pressure P is much higher than the pressure drop in the nozzle and the stress from the supportive matrix[59] and considering the incompressibility of the bioinks, the diameter of printed filaments D is related to the writing speed v_w and the nozzle dimensions (radius R and length L) via $D = \left(\frac{P}{2\eta_0 L \cdot v_w}\right)^{1/2} \cdot R^2$, where η_0 is the viscosity of the bioink at zero shear rate.

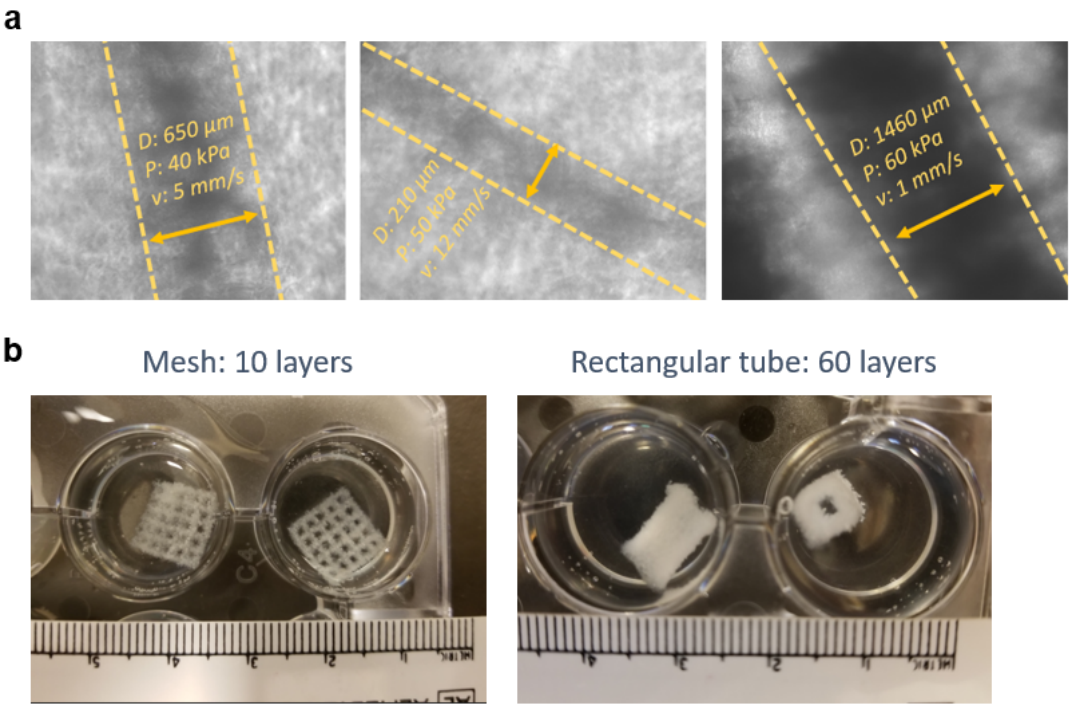

Figure S13 Printed lines and 3D constructs. (a) Filament printed inside PSIM under different combinations of pressure and writing speed. (b) Printed multilayered meshes and rectangular tubes that show cohesion between different layers.

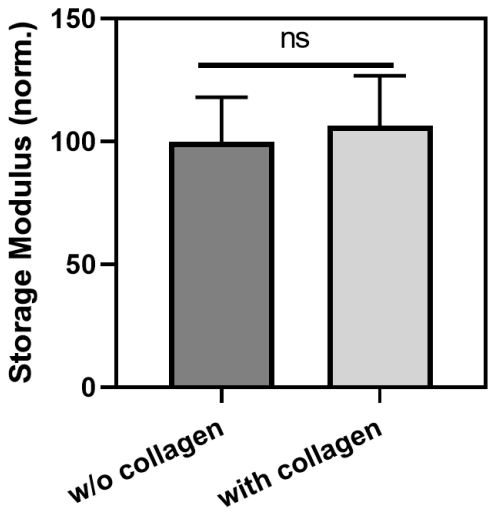

Figure S14 The storage modulus of PEG0 hydrogels with and without 0.02% collagen. Sample size: N=3.

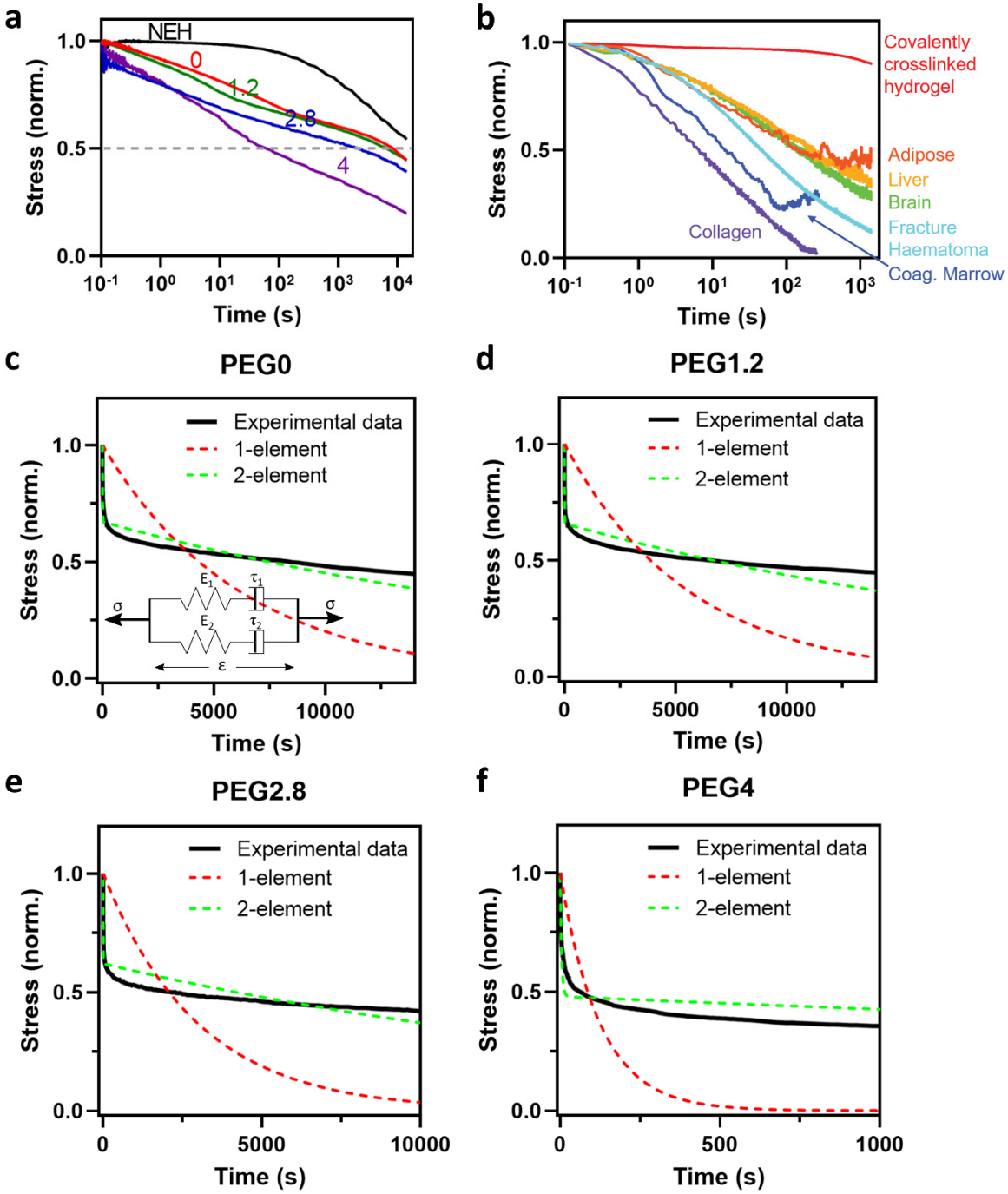

Figure S15 Analysis of stress-relaxation behavior of PVHs with the Maxwell-Wiechert model. (a) Stress relaxation tests on PVHs and NEH. NEH: glyoxal/glycol-chitosan. (b) Stress relaxation behavior of tissues.[8] Reproduced with permission. (c-f) Regression curves of experimentally measured stress relaxation curves (black) of PVHs at pH 6.8 to one- and two-element Maxwell models.

Table S1 Structural and mechanical properties of commonly used bioprinting materials.

	Porosity (%)	Pore size	E (kPa)	$\tau_{1/2}$ (s)	Refs.
PVH	47-71	12-18 μm	1-81	10^2-10^4	—
Chitosan	~ 0	< 100 nm	1-4.5	10^4	[46,60]
Alginate	~ 0	5-17 nm	2.4-72	10^2-10^4	[21,40–42,61]
Gelatin	NA[a)]	12-30 nm	1.5-38.1	10^3-10^4	[51,52,62]
Hyaluronic acid	NA	5.5-12 nm	1.2-105	10^2-10^4	[53,54,63,64]
PEGDA	~ 0	7-25 nm	0.45-168	NA	[5,49,65,66]
Hydroxyethyl methacrylate	~ 0	1.2-8 nm	15-156	10^5	[67–69]
Agarose	NA	85-370 nm	10-140	10^2-10^3	[38,39,70]
Cellulose	< 15.82	20-396 nm	15-59.4	10^2-10^3	[43–45,71,72]
Fibrin	NA	0.6 μm	0.3-5.1	10^3-10^4	[49,50,73]
Silk fibroin	NA	0.5 μm	0.3-90	NA	[74–76]
Collagen	62-64[b)]	1.1-2.2 μm	0.06-1.05	10^0-10^2	[47,48,77]
GelMA	NA	0.2-0.9[b)] μm	3.6-42	NA	[78–80]
GelMA-PEO emulsion	49-68	23-53 μm	2.3-9.8	NA	[15]

[a)]NA, not available from the literature; [b)]Samples prepared by freeze-drying.

Table S2 Regression parameters for stress relaxation data.

PEG conc. (%)	0	1.2	2.8	4
τ_1 (s)	10.57	5.657	1.534	4.548
E_1 (norm.)	0.3287	0.3413	0.3799	0.5207
τ_2	25240	24360	19450	8463
E_2	0.6713	0.6587	0.6201	0.4793

Additional references:

38 P. G. Righetti, B. C. W. Brost and R. S. Snyder, *J. Biochem. Biophys. Methods*, 1981, **4**, 347–363.

39 M. Watase and K. Arakawa, *Bull. Chem. Soc. Jpn.*, 1968, **41**, 1830–1834.

40 T. Boontheekul, H. J. Kong and D. J. Mooney, *Biomaterials*, 2005, **26**, 2455–2465.

41 J. Klein, J. Stock and K. D. Vorlop, *Eur. J. Appl. Microbiol. Biotechnol.*, 1983, **18**, 86–91.

42 O. Chaudhuri, S. T. Koshy, C. Branco Da Cunha, J. W. Shin, C. S. Verbeke, K. H. Allison and D. J. Mooney, *Nat. Mater.*, 2014, **13**, 970–978.

43 S. Sultan and A. P. Mathew, *Nanoscale*, 2018, **10**, 4421–4431.

44 R. Meredith, *J. Text. Inst. Trans.*, 1954, **45**, 438–461.

45 S. Park, R. A. Venditti, H. Jameel and J. J. Pawlak, *Carbohydr. Polym.*, 2006, **66**, 97–103.

46 A. Ghadban, A. S. Ahmed, Y. Ping, R. Ramos, N. Arfin, B. Cantaert, R. V. Ramanujan and A. Miserez, *Chem. Commun.*, 2016, **52**, 697–700.

47 S. Nam, K. H. Hu, M. J. Butte and O. Chaudhuri, *Proc. Natl. Acad. Sci.*, 2016, **113**, 5492–5497.

48 M. Miron-Mendoza, J. Seemann and F. Grinnell, *Biomaterials*, 2010, **31**, 6425–6435.

49 G. P. Raeber, M. P. Lutolf and J. A. Hubbell, *Biophys. J.*, 2005, **89**, 1374–1388.

50 P. A. Janmey, E. J. Amis and J. D. Ferry, *J. Rheol.*, 1983, **27**, 135–153.

51 S. T. Koshy, R. M. Desai, P. Joly, J. Li, R. K. Bagrodia, S. A. Lewin, N. S. Joshi and D. J. Mooney, *Adv. Healthc. Mater.*, 2016, **5**, 541–547.

52 M. Miller, J. D. Ferry, F. W. Schremp and J. E. Eldridge, *J. Phys. Colloid Chem.*, 1951, **55**, 1387–1400.

53 X. Xu, A. K. Jha, D. A. Harrington, M. C. Farach-Carson and X. Jia, *Soft Matter*, 2012, **8**, 3280–3294.

54 J. Lou, R. Stowers, S. Nam, Y. Xia and O. Chaudhuri, *Biomaterials*, 2018, **154**, 213–222.

55 R. F. Potter and A. C. Groom, *Microvasc. Res.*, 1983, **84**, 68–84.

56 J. A. G. Rhodin, *J. Ultrastruct. Res.*, 1968, **25**, 452–500.

57 D. Craiem, F. J. Rojo, J. M. Atienza, R. L. Armentano and G. V. Guinea, *Phys. Med. Biol.*, 2008, **53**, 4543–4554.

58 Z. Liu and K. Yeung, *J. Biomed. Pharm. Eng.*, 2008, **1**, 22–28.

59 Y. Jin, W. Chai and Y. Huang, *Mater. Sci. Eng. C*, 2017, **80**, 313–325.

60 Q. Wu, D. Therriault and M. C. Heuzey, *ACS Biomater. Sci. Eng.*, 2018, **4**, 2643–2652.

61 A. D. Augst, H. J. Kong and D. J. Mooney, *Macromol. Biosci.*, 2006, **6**, 623–633.

62 L. S. Wang, J. Boulaire, P. P. Y. Chan, J. E. Chung and M. Kurisawa, *Biomaterials*, 2010, **31**, 8608–8616.

63 B. Ananthanarayanan, Y. Kim and S. Kumar, *Biomaterials*, 2011, **32**, 7913–7923.

64 J. Lou, F. Liu, C. D. Lindsay, O. Chaudhuri, S. C. Heilshorn and Y. Xia, *Adv. Mater.*, 2018, **30**, 1–6.

65 S. Nemir, H. N. Hayenga and J. L. West, *Biotechnol. Bioeng.*, 2010, **105**, 636–644.

66 S. R. Peyton, P. D. Kim, C. M. Ghajar, D. Seliktar and A. J. Putnam, *Biomaterials*, 2008, **29**, 2597–2607.

67 M. F. Refojo, *J. Appl. Polym. Sci.*, 1965, **9**, 3417–3426.

68 S. Métrailler, École Polytechnique Fédérale de Lausanne, 2012.

69 Z. Mao, D. Yu, W. Liu, B. Wang, X. Zhou and C. Gao, *Soft Matter*, 2012, **8**, 9235.

70 C. T. Buckley, S. D. Thorpe, F. J. O'Brien, A. J. Robinson and D. J. Kelly, *J. Mech. Behav. Biomed. Mater.*, 2009, **2**, 512–521.

71 D. J. McQueen-Mason, Simon J. And Cosgrove, *Plant Physiol.*, 1995, **107**, 87–100.

72 K. Markstedt, A. Mantas, I. Tournier, H. Martínez Ávila, D. Hägg and P. Gatenholm, *Biomacromolecules*, 2015, **16**, 1489–1496.

73 H. Duong, B. Wu and B. Tawil, *Tissue Eng. Part A*, 2009, **15**, 1865–1876.

74 L. Daheron, M. Lovett, G. Vunjak-Novakovic, C. Cannizzaro, D. L. Kaplan and B. Messmer, *Biomaterials*, 2007, **28**, 5271–5279.

75 T. Yucel, P. Cebe and D. L. Kaplan, *Biophys. J.*, 2009, **97**, 2044–2050.

76 Z. Zheng, J. Wu, M. Liu, H. Wang, C. Li, M. J. Rodriguez, G. Li, X. Wang and D. L. Kaplan, *Adv. Healthc. Mater.*, 2018, **7**, 1–12.

77 V. Karageorgiou and D. Kaplan, *Biomaterials*, 2005, **26**, 5474–5491.

78 M. K. Jaiswal, T. Thakur, R. Kaunas, A. K. Gaharwar, E. Cosgriff-Hernandez, J. R. Xavier, N. Sears and P. Desai, *ACS Nano*, 2015, **9**, 3109–3118.

79 X. Li, S. Chen, J. Li, X. Wang, J. Zhang, N. Kawazoe and G. Chen, *Polymers*, 2016, **8**, 269.

80 T. Billiet, E. Gevaert, T. De Schryver, M. Cornelissen and P. Dubruel, *Biomaterials*, 2014, **35**, 49–62.